Int. J. Morphol.,
44(1):325-339, 2026.

Effects of *Paeonia lactiflora* Root Extract on JNK-Mediated Inflammatory Signaling and Cerebral Infarction Reduction in Acute Transient Focal Ischemia in Rats

Efectos del Extracto de Raíz de *Paeonia lactiflora* Sobre la Señalización Inflamatoria Mediada por JNK y la Reducción del Infarto Cerebral en la Isquemia Focal Transitoria Aguda en Ratas

Zhi-Feng Li[1]; Yin-Yin Zhao[2]; Ya-Qian Zhang[3] & Zhuo-Ran Zhu[4]

LI, Z-F.; ZHAO, Y-Y.; ZHANG, Y-Q. & ZHU, Z-R. Effects of *Paeonia lactiflora* root extract on JNK-mediated inflammatory signaling and cerebral infarction reduction in acute transient focal ischemia in rats. *Int. J. Morphol., 44(1)*:325-339, 2026.

SUMMARY: Cerebral ischemia-reperfusion (CI/R) injury significantly endangers cognitive abilities following a cerebral infarction (CI). This research investigated the impact of *Paeonia lactiflora* L. root extract (PLRE) on a CI/R model using Wistar rats, along with the mechanisms involved. A total of fifty Wistar rats were randomly assigned to five groups: a control group, a group supplemented with 50 mg/kg of PLRE, a CI group, and two CI groups treated with 25 mg/kg and 50 mg/kg of PLRE, each consisting of 10 rats. Cognitive function was evaluated through the Y-maze test. Furthermore, we utilized enzyme-linked immunosorbent assay (ELISA) and real-time PCR to analyze the expression of genes linked to JNK-mediated TLR4/T3JAM- and ASK1-related apoptosis and inflammatory signaling in the brain. Compared to the control group, the CI group showed a significant delay in maze completion ($p<0.05$). This group also exhibited markedly higher levels of pro-inflammatory cytokines, along with decreased levels of anti-inflammatory cytokines and neurotrophic growth factors [brain-derived neurotrophic factor (BDNF) and glial cell line-derived neurotrophic factor (GDNF)] ($p<0.05$). Conversely, the group treated with 50 mg/kg PLRE post-CI showed improvements, including reduced electrical stimulation time, elevated levels of neurotrophic growth factors, and a beneficial alteration in the expression profiles of genes related to inflammation and apoptosis (such as glucose-regulated protein 78 (GRP78), activating transcription factor 6 (ATF-6), TLR4, T3JAM, and ASK1) compared to the CI group ($p<0.05$). These findings indicate that the PLRE extract may alleviate cognitive deficits following CI in rats, possibly by modulating inflammatory factors secreted by microglia.

KEY WORDS: *Paeonia lactiflora* L.; Cerebral infarction; Apoptosis; Cerebral ischemia-reperfusion.

INTRODUCTION

Cerebral stroke (CS) is a significant global health issue, recognized as one of the leading causes of mortality and long-term disability. The condition arises from an interruption in blood flow to the brain, leading to rapid neuronal cell death. Ischemic strokes, which account for approximately 85 % of all stroke cases, typically result from blood clots obstructing cerebral arteries. In contrast, hemorrhagic strokes occur due to the rupture of blood vessels (Kim *et al*., 2020). Various risk factors contribute to the incidence of ischemic strokes, including advanced age, hypertension, and diabetes. The impact of ischemic strokes is profound, often resulting in immediate neurological decline and persistent disabilities that affect patients' quality of life (Owolabi *et al*., 2021). The pathophysiology of ischemic stroke involves excessive production of reactive oxygen species (ROS), which induces oxidative stress, apoptosis, and cell death during ischemia-reperfusion injury (CIS/R). The fundamental mechanisms of damage during these events include excitotoxicity and inflammatory responses, primarily mediated by pro-inflammatory cytokines such as interleukin-1 beta (IL-1β) and tumor necrosis factor-alpha (TNF-α) (Yuan *et al*., 2021). Current therapeutic options are limited, with aspirin and thrombolytic agents being the primary treatments available for select patients. Despite significant advancements in understanding the underlying mechanisms of CS and CIS/R, effective

[1] Department of Orthopedics, Taihe Hospital, Hubei University of Medicine, Shiyan, China.
[2] Department of Gynecology and Obstetrics, Taihe Hospital, Hubei University of Medicine, Shiyan, China.
[3] Fukang Community Hospital, Hubei University of Medicine, Shiyan, China.
[4] Department of Anatomy, Basic Medical College, Hubei University of Medicine, Shiyan, China.

Received: 2025-10-18 Accepted: 2025-11-23

therapeutic strategies remain elusive, often hampered by severe side effects, narrow treatment windows, and additional damage incurred during reperfusion. However, recent animal studies have demonstrated potential in targeting these pathways to mitigate brain injury and improve outcomes (Zhang *et al*., 2023).

The intricate interplay of cellular mechanisms involved in CS and CIS/R encompasses apoptosis, neurotrophic factors, and stress responses. Apoptotic pathways, including those mediated by Bax, Bcl-2, p53, and caspase-3, play critical roles in regulating neuronal death. Research utilizing rodent models has shown that manipulation of these pathways—such as enhancing Bcl-2 expression or inhibiting p53—can significantly reduce brain damage (Kulshrestha *et al*., 2019). Furthermore, neurotrophic factors like brain-derived neurotrophic factor (BDNF) and glial cell line-derived neurotrophic factor (GDNF) are essential for neuronal survival and recovery following a stroke, with therapies aimed at upregulating these factors showing promise in preclinical studies (Tunca *et al*., 2014). In this context, GRP78, an endoplasmic reticulum (ER) chaperone protein, emerges as a protective factor against ER stress, facilitating proper protein folding and preventing apoptosis. Studies on rodent models of ischemic stroke have indicated that GRP78 expression is upregulated as a protective response, and enhancing its levels may reduce neuronal apoptosis and infarct size, highlighting its potential as a therapeutic target. Additionally, the transcription factor ATF-6, activated during ER stress, promotes the expression of protective genes such as GRP78 (Ni *et al*., 2011). The modulation of ATF-6 has been associated with influencing the extent of brain injury following CIS/R, suggesting that targeting this pathway may offer new therapeutic avenues for mitigating ER stress-related damage in stroke. Overall, rodent models have proven invaluable for elucidating these complex pathways and exploring potential therapeutic strategies, including antioxidants and neurotrophic factor therapies, to address CIS/R-induced brain injury (Liang *et al*., 2024).

Post-ischemic inflammation is a critical component of stroke pathology, particularly during the early phases of cerebral ischemia-reperfusion (I/R) injury. The initial increase in free radical production and subsequent oxidative stress in the ischemic region triggers inflammatory responses (Meng *et al*., 2019). This inflammation is predominantly mediated by microglia, astrocytes, and necrotic cells, which release pro-inflammatory mediators that exacerbate cerebral I/R injury. Toll-like receptor (TLR)-mediated signaling pathways play a pivotal role in initiating these inflammatory cascades, which are closely linked to the development of cerebral infarction. TLR4, a key member of the TLR family, is expressed on microglia and astrocytes within the ischemic area during cerebral I/R injury. Upon brain ischemic insult, activated microglia and reactive astrocytes predominantly express TLR4, recognizing damage-associated molecular patterns (DAMPs) and triggering downstream signaling cascades through myeloid differentiation primary response gene 88 (MyD88)-dependent and toll/interleukin (IL)-1 receptor homology domain-containing adaptor-inducing interferon-b (TRIF)-dependent pathways (Li *et al*., 2014). These pathways lead to the activation of the transcription factor nuclear factor-kappa B (NF-κB), which subsequently stimulates the production of various pro-inflammatory mediators (Yu *et al*., 2020). Notably, the expression of TLR4, ionized calcium-binding adapter molecule 1 (Iba1), and glial fibrillary acidic protein (GFAP) significantly increases in the ischemic area within 24 hours following transient focal cerebral ischemia. The MyD88-dependent signaling pathway activates NF-κB and mitogen-activated protein kinase (MAPK) pathways, including JNK, while TRIF-dependent signaling activates interferon-β expression, amplifying the inflammatory response (Su *et al*., 2018). The activation of JNK signaling is particularly noteworthy, as it plays a crucial role in mediating neuroinflammation and apoptosis in response to I/R injury in both in vitro and in vivo models (Ma *et al*., 2025).

The activation of JNK pathways during cerebral ischemia occurs through various stimuli, including TLR4/MyD88/TRAF6-, TLR4/T3JAM-, and ASK1-mediated signaling. Phosphorylated JNK positively regulates activated NF-κB, promoting its translocation to the nucleus and inducing the expression of pro-inflammatory cytokines such as inducible nitric oxide synthase (iNOS), cyclooxygenase-2 (COX-2), TNF-α, and IL-6 (Cheng *et al*., 2021). These inflammatory cascades contribute to the exacerbation of oxidative stress and the disruption of the blood-brain barrier (BBB), ultimately worsening cerebral infarction. COX-2, an inducible isoform of cyclooxygenase, is particularly relevant in this context as it is highly expressed in the ischemic area and promotes microglial activation, leading to an increased infarct size. Elevated levels of TNF-α further compromise BBB integrity and stimulate iNOS production, creating a vicious cycle that amplifies the inflammatory response and exacerbates brain injury (Xu *et al*., 2021). IL-6, primarily produced by activated microglia, is also implicated in BBB disruption and neuronal damage, peaking in expression during the ischemic penumbra following transient middle cerebral artery occlusion (MCAO). Given the complexities of these inflammatory pathways, there is growing interest in traditional herbal medicines, which offer multi-target capabilities and synergistic effects that may provide advantages over conventional single-target approaches (Mohsen *et al*., 2021; Zhu *et al*., 2023).

Paeonia lactiflora L. root extract (PLRE), derived from a plant in the Paeoniaceae family, has garnered attention for its potential therapeutic properties. Native to Eastern Europe, Asia, and Northern Africa, PLRE thrives in humid regions and is characterized by its pinkish-white flowers (Kim *et al*., 2021). Rich in bioactive compounds, PLRE has been traditionally used in Asia for treating various ailments, including ischemic heart diseases, where it exhibits anti-inflammatory and antioxidant effects (Wen *et al*., 2023). Recent studies indicate that PLRE may protect against cerebral I/R injury by modulating JNK-mediated signaling pathways, making it a promising candidate for further investigation in the context of acute transient focal ischemia (Choi *et al*., 2023). This study aims to assess the effects of PLRE on cerebral infarction and elucidate the underlying mechanisms by which it modulates JNK-mediated inflammatory signaling in the penumbral cortex following transient MCAO.

MATERIAL AND METHOD

Preparation of PLRE

Fresh roots of *Paeonia lactiflora* L. (2000 grams) were initially dried at 40 °C in a dark environment after being verified by a botanist. The dried roots were then finely ground using a soil grinder. This resulting powder was combined with a 70:30 ethanol/acetone solution (v/v) and incubated at 42 °C for 72 h. After incubation, the mixture was filtered through paper and concentrated using a rotary evaporator. The final extract of *Paeonia lactiflora* root (PLRE), weighing 590 grams, was stored at 4 °C (Khazaei *et al*., 2023).

Liquid Chromatography-Mass Spectrometry (LC–MS/MS) of PLRE

For the analysis of PLRE using Liquid Chromatography-Mass Spectrometry (LC–MS/MS), two grams of the PLRE powder were dissolved in 100 mL of absolute methanol. The solution was then subjected to ultrasonic shaking at room temperature for 30 minutes. Following this, the solution was filtered, and the filtrate was collected as the sample solution. Mass spectrometric characterization was carried out using an Agilent G6410 Triple Quadrupole system linked to a Bruker HCTultra ion trap mass spectrometer via negative electrospray ionization (ESI-). Chromatographic separation utilized a Zorbax SB-C18 column (150 mm × 2.1 mm, 3.5 μm) maintained at 25 °C, with a flow rate of 0.3 mL/min using acidified mobile phases: A (0.1 % acetic acid in water) and B (0.1 % acetic acid in acetonitrile). The gradient program over 75 min began with 10 % B, increasing to 50 % from 0 to 25 min, then to 95 % from 25 to 45 min, followed by a 10-minute hold at 95 %, a transition to 100 % B from 55 to 60 min, and a final hold at 100 % from 60 to 75 min. Mass spectrometry parameters included a capillary voltage of 4 kV, nebulizer pressure at 15 psi, nitrogen drying gas flow at 6 L/min, a capillary temperature of 300 °C, and a scan range of 130–1100 m/z. The mobile phase flow rate was set at 1.0 mL/min, with a total run time of 85 min. The effluent was monitored using a photodiode array detector at 254 nm. Prior to analysis, a predefined compound library containing exact masses (±5 ppm) and retention times (±0.5 min) was validated against certified reference standards (Soleimani *et al*., 2025).

Transient middle cerebral artery occlusion (MCAO)

For the transient middle cerebral artery occlusion (MCAO) procedure, rats underwent the intraluminal suture occlusion technique as previously described. Initially, all rats were anesthetized with isoflurane, using 5 % for induction and 2 % for maintenance. The rat's head was secured in a stereotaxic frame, and a burr hole was drilled into the skull, positioned 2.0 mm posterior and 2.5 mm lateral to the right of the bregma, to expose the distal region of the middle cerebral artery (MCA). A midline neck incision of 3 cm was made to access the right external carotid artery (ECA) and internal carotid artery (ICA). A 3–0 nylon suture with a heat-blunted tip was carefully inserted into the lumen of the right ICA through the stump of the ECA and advanced to the origin of the MCA. After maintaining occlusion for 90 min, the suture was gently retracted to allow for reperfusion. Blood flow in the MCA was continuously monitored using Laser-Doppler flowmetry (DRT4, Moor Instruments Inc., Wilmington, USA) during the MCAO procedure. Successful MCAO was defined by a reduction in MCA blood flow to 20–30 % of baseline during the ischemic phase and an increase to 60 % of baseline during reperfusion. Rats that experienced incomplete MCAO were excluded from further studies (Sun *et al*., 2023).

Experimental design and research time line

Fifty male Wistar rats, each weighing 190±30 g, were randomly assigned to five groups, with ten rats per group. Prior to the commencemen2t of the study, the rats underwent a 72-hour acclimatization period to adapt to the environmental conditions, which included temperature, food, and water availability. They were housed in propylene cages maintained at a temperature of 26±2 °C and a relative humidity of 35±3 %, under a 12-hour light/dark cycle, with free access to standard pellets and tap water. All animal care and euthanasia procedures received approval from the Hubei University of Medicine ethics committee and adhered strictly

to established protocols for laboratory animal welfare. The sham group and the ischemic stroke-reperfusion (IS/R) group were given intraperitoneal injections of 0.5 mL of phosphate-buffered saline (PBS). The co-treatment groups (IS/R +25 and IS/R +50 PLRE) received oral doses of 25 mg/kg and 50 mg/kg of PLRE, respectively, while the sham +400 PLRE group was administered 50 mg/kg of PLRE orally. The non-toxic effective dose was determined using the LD50 method, along with preliminary studies and existing literature on PLRE. PLRE was administered daily at a consistent time (9 AM) for a duration of 50 days. During the procedures, the rats were kept under anesthesia with 2 % isoflurane, and a burr hole was drilled into the right side of the skull, positioned 0.8 mm posterior to the bregma and 1.5 mm lateral to the midline. An intracerebroventricular (ICV) injection of 10 mL of SP600125 solution (2 mM in DMSO, ab120065, Abcam) or a 1 % DMSO solution was delivered at a depth of 3.5 mm from the skull using a 10-μL Hamilton syringe (Cheng *et al*., 2021; Kim *et al*., 2021).

LD50 for PLRE

The LD50 of PLRE was evaluated using Lork's two-step procedure. Initially, nine rats were divided into three groups and administered PLRE at doses of 30, 300, and 3000 mg/kg. These animals were closely monitored for any signs of mortality or toxicity over a 24-hour period. Following this initial assessment, an additional set of three rats per group received PLRE at doses of 10, 100, and 1000 mg/kg, with similar monitoring for any adverse effects. The LD50 was calculated using Lork's formula, which determines the median lethal dose based on the lowest dose that caused mortality (D lethal) and the highest dose that did not result in observed mortality (D normal). The formula used for this calculation is:

$$\text{LD50 of PLRE} = (\text{D normal} \times \text{D lethal})^{1/2}$$ (Khordad *et al*., 2024).

Morris water maze test

The Morris water maze test, a widely recognized method for assessing spatial learning and memory, was conducted in this study from day 20 to day 40 following ischemic stroke-reperfusion (IS/R). The maze consisted of a circular tank measuring 120 cm in diameter and 50 cm deep, placed in a quiet, dark room with distinct visual cues. The water temperature was maintained at 23 ± 4 °C. A black, round platform (10 cm in diameter) was submerged 2 cm below the water's surface in a fixed location at the center of one quadrant throughout the training phase. Swimming paths of the rats were recorded using a video camera connected to a computer, and the data were analyzed with image processing software. Each rat underwent training twice daily for five consecutive days, starting from one of four randomly assigned points in the pool. The escape latency, or the time taken for the rat to locate the hidden platform, was recorded, with a maximum time limit of 90 seconds. If a rat failed to find the platform within this period, it was guided to the platform and allowed to remain there for 15 seconds, with its escape latency noted as 90 seconds. One day after the final training session, the platform was removed, and a 90-second probe test was conducted to evaluate memory retention, during which the frequency of rat crossings over the area where the platform had been previously located was recorded (Zhang & Dong, 2024).

Glutathione peroxidase (GPx), Catalase (CAT), and Superoxide dismutase (SOD) serum activity

We utilized a sandwich ELISA kit specifically designed for rodents, supplied by Cusabio (China), to quantify serum levels of superoxide dismutase (SOD), catalase (CAT), and glutathione peroxidase (GPx). The specific catalog numbers for the kits used were CSB-EL022397RA for SOD, CSB-E13439r for CAT, and CSB-E12146r for GPx. The assay was conducted following the manufacturer's instructions to ensure accuracy and reliability (Zhang & Dong, 2024).

Serum levels of nitric oxide (NO)

To evaluate serum nitric oxide (NO) levels, which serve as critical indicators of lipid peroxidation and oxidative stress, we employed the Griess colorimetric method. In this procedure, 500 mL of serum samples were mixed with 6 mg of zinc oxide, thoroughly combined, and then centrifuged at 10,000 g for 15 min to separate the components. The resulting supernatant was then combined with 500 μL of Griess reagent. Following this, the mixture was incubated for 60 min at 37 °C to allow for the development of color. The absorbance of the solution was subsequently measured using a Stat Fax ELISA reader (303 microwell reader, Awareness Technology, USA) at wavelengths of 540 nm and 630 nm. This method provided a reliable assessment of nitric oxide levels in the serum, reflecting the oxidative stress status of the subjects (Ma & Wang, 2025).

Brain tissue thiol, lipid peroxidation levels [thiobarbituric acid reactive substances (TBARS)], and total antioxidant capacity (FRAP levels) levels

To determine thiol levels, an important antioxidant marker, 100 μL of homogenized brain tissue was combined with 20 μL of 5,5'-dithiobis-(2-nitrobenzoic acid) (DTNB). The mixture was incubated at 37 °C for 15 min and then centrifuged at 12,000 g for 5 min. The absorbance of the

supernatant was measured at 412 nm with an ELISA reader. These assays collectively provided insights into the oxidative status and antioxidant capacity of the brain tissue.

Lipid peroxidation levels were evaluated by quantifying thiobarbituric acid reactive substances (TBARS) in the brain tissue. For this, 100 μL of the homogenized brain tissue was mixed with 100 μL of TBARS solution and incubated at 37 °C for 30 min. The mixture was then centrifuged at 12,000 g for 5 min, and the absorbance of the supernatant was recorded at 593 nm using an ELISA reader.

To assess the total antioxidant capacity, we utilized the Ferric Reducing Ability of Plasma (FRAP) assay. In this process, 100 mg of brain tissue was homogenized at 4 °C and mixed with 200 μL of cold phosphate-buffered saline (PBS). A 100 μL aliquot of this homogenate was then combined with 10 μL of FRAP reagent. Following a 15-minute incubation at 25 °C, the mixture was centrifuged at 12,000 g for 10 minutes, and the absorbance of the resulting supernatant was measured at 593 nm using a Stat Fax ELISA reader (303 microwell readers, Awareness Technology, USA) (Zhang & Dong, 2024).

Serum concentrations of GDNF, BDNF, TNF-α, IL-4, IL-1β, IL-10, and IL-6

To assess the anti-inflammatory effects of PLRE, we measured the levels of various cytokines utilizing rodent-specific sandwich ELISA kits from Novus Biologicals (USA). Specifically, we quantified the anti-inflammatory cytokines interleukin-10 (IL-10, Cat. No.: R1000) and interleukin-4 (IL-4, Cat. No.: NBP1-91171), as well as pro-inflammatory cytokines including interleukin-1 beta (IL-1β, Cat. No.: RLB00), tumor necrosis factor-alpha (TNF-α, Cat. No.: NBP2-DY410), and interleukin-6 (IL-6, Cat. No.: M6000B), adhering to the provided protocols.

Serum was collected by centrifuging the blood at 10,000 g for 20 min. The levels of glial cell line-derived neurotrophic factor (GDNF, Cat. No.: ab244211) and brain-derived neurotrophic factor (BDNF, Cat. No.: ab108319) in the serum were quantified using ELISA kits from Abcam (USA). The assays were performed following the manufacturer's guidelines and protocols (Yang *et al*., 2026).

Brain tissue glucose-regulated protein 78 (GRP78), activating transcription factor 6 (ATF-6), JNK, TLR4, T3JAM, and ASK1

Total RNA was extracted using Trizol, following the manufacturer's instructions (Ambion, China). Five micrograms of the isolated RNA were then reverse transcribed into complementary DNA (cDNA) using random primers. Quantitative real-time PCR was conducted with SYBR Green (Vazyme, China) on an ABI7900 fluorescence PCR system (CA, USA). The PCR cycling conditions were established as follows: 2 min at 50 °C, 10 min at 95 °C, followed by 40 cycles of 30 s at 95 °C and 30 s at 60 °C. Gene expression levels were normalized to glyceraldehyde-3-phosphate dehydrogenase (GAPDH). The primer sequences utilized in the study were as follows:

GAPDH: Forward: TGAAGGTCGGAGTCAACGG; Reverse: AGAGTTAAAAGCAGCCCTGGTG
GRP78: Forward: ATGAGTCCACACCCAGAA; Reverse: TCACTGCGGATAGCAGAG
JNK1: Forward: GCCGAGGATGATGAGGAGG; Reverse: TCTCCAGCCATGATGGGTT
TLR4: Forward: CTGCTGCTGCTGCTGCTG; Reverse: GCTGCTGCTGCTGCTGCTG
T3JAM: Forward: GCCACCTGCTGCTGCTG; Reverse: GCTGCTGCTGCTGCTG
ASK1: Forward: GCCAGCAGTCTCAGTCTTCA; Reverse: GCTGCTGCTGCTGCTGCTG
ATF-6: Forward: ATGAGCGGATCCGCGAGAC; Reverse: TCAGGAGCAGCTGTTGTCCT

Relative gene expression levels were calculated using the threshold cycle (Ct) method, along with the DDCt method and fold change formulas.

The fold formula change = $2^{-\Delta\Delta CT}$; ΔΔCt = [(Ct sample - Ct GAPDH gene) - (Ct sample – Ct control)] (Khazayel *et al*., 2025).

Brain stereology and histopathology

In this study, methylene blue and Golgi's staining staining was employed to examine brain tissue, emphasizing neuronal structures and cellular details. The brain tissues were initially fixed in 10 % paraformaldehyde for 24 to 48 hours, followed by washing with phosphate-buffered saline (PBS). The samples were then dehydrated through a series of graded ethanol solutions and cleared using xylene or an alternative clearing agent. Subsequently, the samples were embedded in paraffin and sectioned into 5-10 μm slices using a microtome (LEICA SM2010RV1.2, Germany). The sections were rehydrated and stained with a 1 % methylene blue solution for 10 to 20 min. After staining, the sections were rinsed in PBS, re-dehydrated, cleared, and mounted with a mounting medium and coverslip. The classical Golgi impregnation technique involves sequential immersion of fresh brain tissue sections in a potassium dichromate ($K_2Cr_2O_7$) solution followed by silver nitrate ($AgNO_3$) treatment, typically maintaining a 1:3 molar ratio over 24-

48 hours to facilitate silver chromate crystal formation within neuronal processes. Post-incubation, specimens undergo thorough washing in deionized H_2O to remove unbound ions, followed by graded ethanol dehydration (70 % → 95 % Æ absolute) to achieve complete water displacement. Tissues are then immersed in xylene as a clearing agent before being infiltrated with molten paraffin wax (56-58 °C) for 4-6 h. The embedded blocks are microtome-sectioned at 4-6 mm thickness and mounted on pre-treated glass slides using albumin-based adhesive, preserving the metallic precipitate distribution critical for visualizing neuronal arborization patterns under light microscopy. Histological analysis was performed using a light microscope at ×100 and ×400 magnifications. Images were captured using a BX61TRF calibrated light microscopy system (Olympus, Japan) and processed with ImageJ software. To calculate the relative volume (Vv) of specific brain structures (total, neuronal paranchymal tissue, blood vessels, ventricles, and areas of focal ischemia), a point probe method was utilized. This was conducted using a Nikon light microscope equipped with Kecam (Kecam Technologies) and TopView software (Version 3.7). The images were processed with Adobe Photoshop CC (Adobe Systems). The relative volume was calculated by multiplying the point density by the reference volume for each structure. A total of 50 points were used for calculating the volumetric density of the brain, with the total number of points located on each structure counted in each field of view and compared to the total number of points in the volume measurement formula: Vv = ∑Pstructure/ ∑Preferenc (Fig. 1a-f) (Khazayel *et al*., 2025).

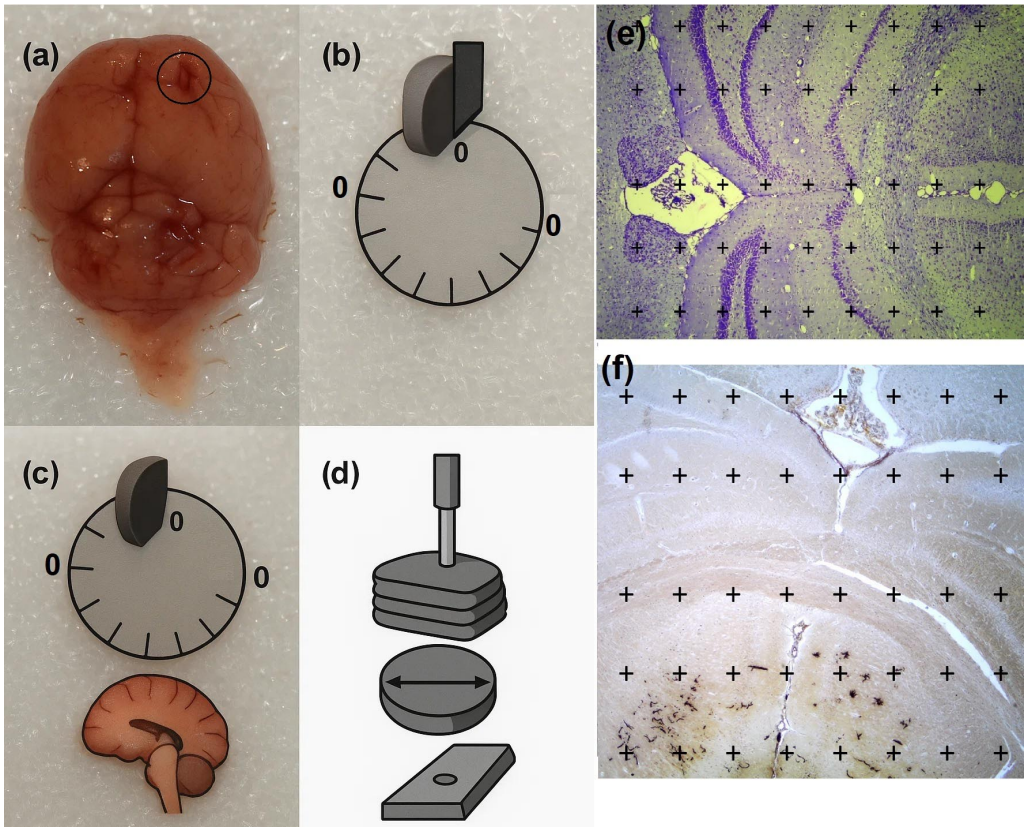

Fig. 1. (a) Rat brain gross tissue with focal ischemic area (in circle). (b) Orientator method for generating isotropic uniform random sections. Each rat brain was placed on a circle of which each was divided into 10 equal distances (u-clock). A random number between 0 and 10 was selected, and the brain was sectioned into two halves using a blade in that direction (here 3). (b) The cut surface of the one half of the brain was placed vertically on the h-clock with 10 unequal sinus-weighted divisions. The second cut done by selecting a random number (here 9). (c) The cut surface of the other half of the brain was then placed parallel to the 0–0 direction of the h-clock and the second cut done by selecting a random number (here 3). The entire brain was sectioned into slabs with a blade placed in the direction of the second cuts between 7 and 10 slabs were obtained from the brain. (d) A trocar was used to punch a circle from a brain slab. The diameters of the circular piece of the brain and the area of the circle were then estimated. (e) and (f) Point probe (50 points) to estimate the volume density of all structures. A total of 50 points were used for calculating the volumetric density of the brain, with the total number of points located on each structure counted in each field of view and compared to the total number of points in the volume measurement formula: Vv = ∑P structure /∑P reference.

Transmission electron microscopic (TEM) study

For transmission electron microscopy (TEM) analysis, brain tissue specimens (1 mm^3) underwent initial fixation in phosphate-buffered 1.5 % glutaraldehyde for 72 hours, followed by post-fixation treatment with 2 % osmium tetroxide for 90 min. Sequential ethanol dehydration (70-100 % gradient) preceded the preparation of semi-thin sections (0.2-0.4 μm thickness) that were toluidine blue-stained for light microscopic identification of target regions. Selected areas were then ultrathin-sectioned (80 nm) and dual-stained with uranyl acetate and lead citrate solutions before being imaged under a JEOL-JEM-100 SX electron microscope (80 kV acceleration voltage) equipped with an iTEM MegaView digital imaging system (Goodarzi *et al*., 2021).

Statistical analysis

The normality of all data was assessed using the Kolmogorov-Smirnov test with a significance level set at 0.05. All numeric data, except for neurological function scores, were found to follow a normal distribution ($P > 0.05$). The results are presented as mean ± standard deviation (SD) and were analyzed using one-way analysis of variance (ANOVA), followed by a Bonferroni post-hoc test. For neurological function scores among the experimental groups, data were analyzed using the Kruskal-Wallis one-way ANOVA, and the results are expressed as median (minimum-maximum). P values less than 0.05 were considered statistically significant.

RESULTS

LD50 of PLRE

After a 24-hour observation period for the groups treated with PLRE, it was determined that the safe dose (D normal) was 1000 mg/kg, while the toxic dose (D lethal) was identified as 3000 mg/kg. Utilizing Lork's formula, the LD50 for PLRE was calculated to be 1732 mg/kg. This indicates that doses below this LD50 value are suitable for use in animal studies.

LC-ESI/MS analysis

LC-ESI/MS was employed to comprehensively characterize the compounds present in the PLRE extracts. In negative ion mode, 41 compounds and 56 peaks were identified. The resulting chromatograms indicate that the hydroalcoholic PLRE extract was analyzed. A full MS scan was first collected as a total ion current chromatogram (TIC), after which reconstructed ion chromatograms (RICs) were created for each anticipated [M-H]- ion based on the expected molecular weights of the potential constituents. Following chromatogram processing, the extracts were separated according to the molecular weight [M-H]- of the target phenolic compounds and their acquisition times. The table lists the counts (Mass-to-Charge, ×104) and the EIC peak counts (acquisition time, ×105) (Fig. 2, Table I).

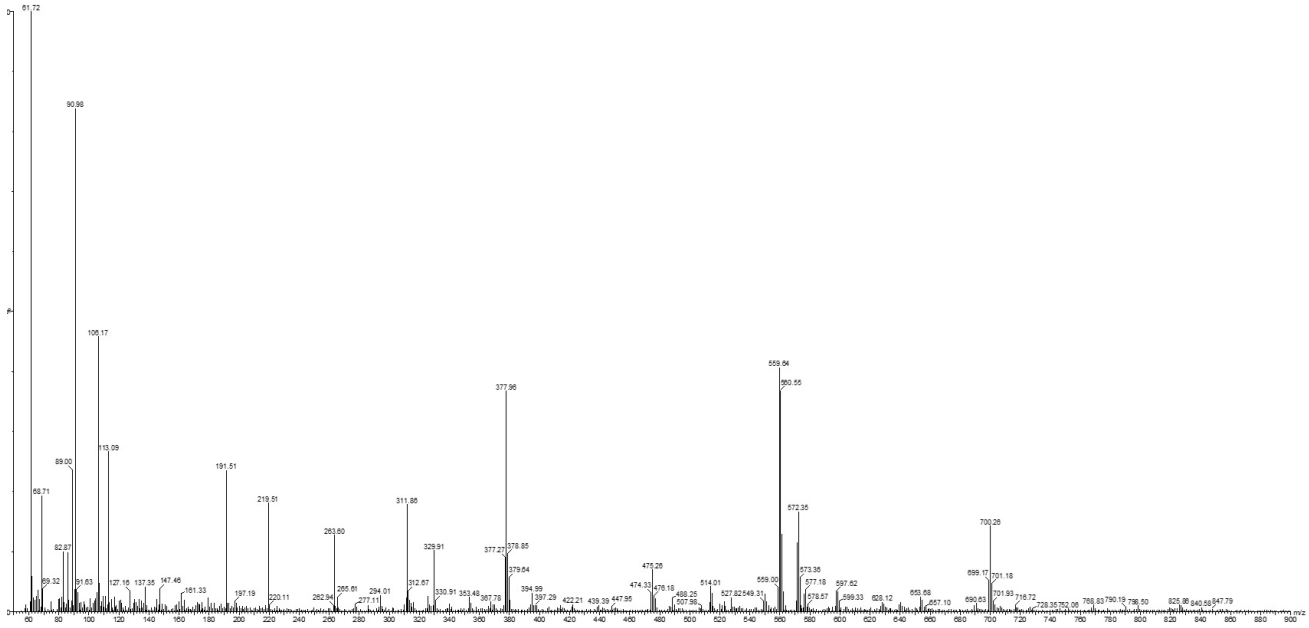

Fig. 2. Chromatogram analyses by LC-ESI/MS of PLRE.

Table I. Qualitative analyses by LC-ESI/MS of PLRE.

Compound	M/Z $(M-H)^-$	MS/MS fragments	Acquisition time	Counts (Mass-to-charge) $x10^4$
3-O- (Z)-p-Coumaroylquinic acid (337)	337	337	1.72	4.8
Caffeic Acid (179)		306		
		179		
Rosmarinic acid derivative (365)	365	191	2.2	93.2
		179		
Furanic compounds (furfural derivates) (91)	90.95	90.95	7.56	8.23
p-Hydroxyacetophenone (137)		137		
Dihydroxybenzophenone derivative (159)		159		
Protocatechuic acid (159)	159	159	9.19	159.35
Naringenin derivates (273)		273		
Esculin (341)		341		
Coumaric acid-O-pentoside (295)	295	295	10.3	23.4
Kaempferol galloylglucoside (599)		599		
Quercetin-3,7-diglucoside (625)		625		
Kaempferol-3,7-di-O-glucoside (609)	609	609	10.7	49.2
Formononetin (267)	267	267	12.3	8.6
Genistein (268)		268		
Biochanin A-7-glucoside (445)	445	445	12.6	6.8
Formononetin (267)		267		
		268		
		677		
Biochanin A (283)	283	283	12.91	23.4
Ophiopogonanone A (327)		327		
Daidzein 7-O-beta-D-glucoside (417)		417		
Epimedoside A (663)		487		
		501		
		663		
Apigenin-7-O-glucoside (431)	431	431	13.5	11.22
Hesperetin (301)		265		
		301		
		227		
		265		
Dihydrocaffeoyl glycerol (219)	219	219	13.9	12.12
Isoferuloyl glycerol (263)		263		
Formononetin (267)	267	267	14.1	37.2
		795		
Malvidin (331)	331	331	14.6	4.06
Ethyl gallate (197)		197		
		307		
Apigenin 6,8-diglucoside (593)	593	593	14.8	3.58
Galloyl-HHDP-hexoside (633)		309		
		633		
		795		
Kaempferol-3-O-sophoroside-7-O-glucoside (777)	777	592	15	5.36
Coumaric acid-*O*-rhamnoside (309)		777		
Protocatechuic acid derivate (91)	91	91	15.9	3.31
		106		
Biochanin A (283)	283	283	15.3	648.6
		675		
Paeoniflorin (480)	540	540	17	6.52
Genistein 8-C-glucoside-xyloside (311)		197		
Quercetin-3-O-pentoside (433)		219		
		311		
Methyl digallate (329)	329	329	20.24	1.48
Bergenin (331)		331		
4-Hydroxybenzoic acid (137)		137		

Compounds characterized for the first time by LC-ESI-MS/MS (intensity> 5¥104). The identification was confirmed by direct comparison with standard compound, respectively.

PLRE improved IS/R -induced spatial cognitive deficits

PLRE administration mitigated IS/R-induced spatial cognitive deficits, as demonstrated through Morris water maze testing following 50 days of treatment. During training, while all groups showed progressive reductions in escape latency, the normal group significantly outperformed the IS/R group from day 4 onward ($p < 0.05$). Although IS/R + PLRE (25/50 mg/kg) groups exhibited longer latencies than normal controls on days 4-5 ($p < 0.05$), their performance remained comparable to the IS/R group ($p > 0.05$), suggesting PLRE's dose-dependent learning enhancement. In the probe test, the IS/R + 50 mg/kg PLRE group showed significantly more platform-area crossings than untreated IS/R rats ($p < 0.05$), indicating preserved spatial memory. These findings collectively demonstrate that 50 mg/kg PLRE effectively counteracts both learning impairments during training and memory deficits in retention testing caused by IS/R (Figs. 3a & 3b).

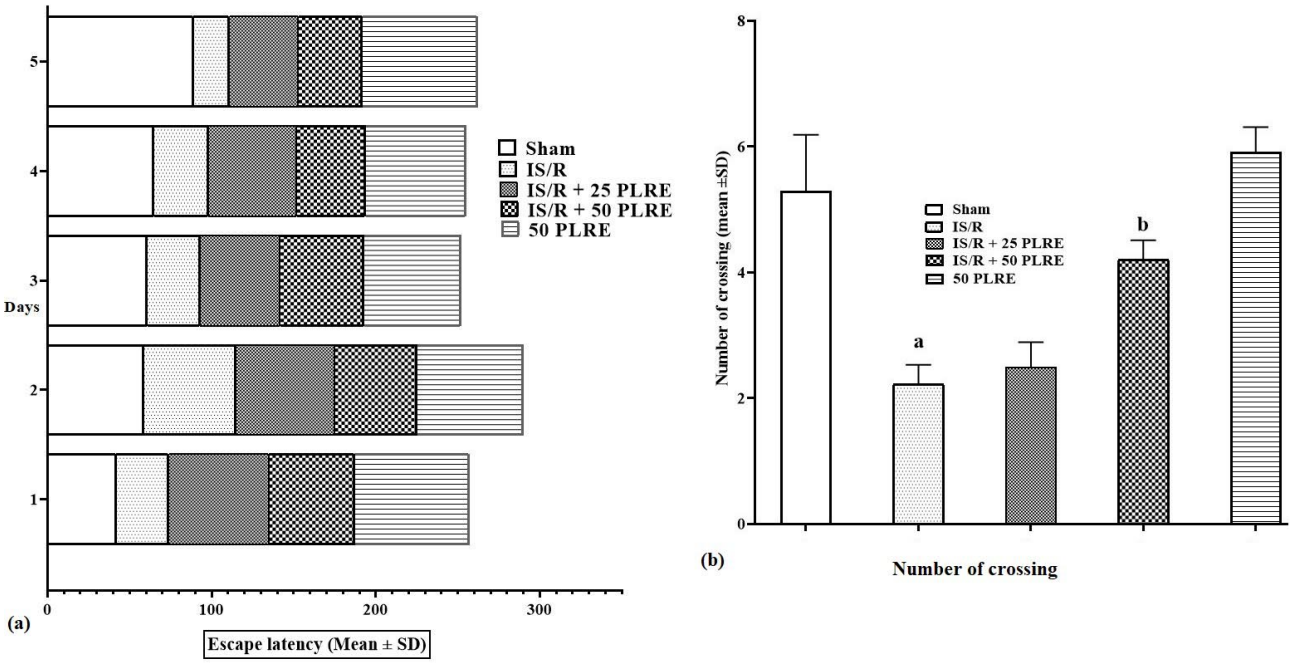

Fig. 3. Morris water maze performance metrics: (a) Platform crossings during probe trial and (b) Escape latency during acquisition phase (mean ± SD; n=10/group). Data demonstrate that IS/R injury significantly impaired spatial memory retention (ap<0.05 vs. sham group, one-way ANOVA with Tukey's post-hoc) while both PLRE treatment doses (25/50 mg/kg) showed dose-dependent recovery of cognitive function (bp<0.05 vs. IS/R group).

PLRE and IS/R effects on serum concentrations of GDNF and BDNF

IS/R was found to suppress the brain's secretion of neurotrophic factors by activating apoptotic pathways in glial cells, leading to a significant reduction ($p < 0.05$) in serum GDNF and BDNF levels relative to the sham group. Conversely, PLRE treatment at both doses increased serum GDNF and BDNF concentrations, highlighting PLRE's strong ability to support and protect glial cells. Notably, the IS/R + 50 mg/kg PLRE group showed a significant rise ($p < 0.05$) in GDNF and BDNF levels compared with the IS/R group (Fig. 4a).

PLRE and IS/R effects on serum concentrations of TNF-α, IL-4, IL-6, IL-10, and IL-1β

IS/R-triggered inflammatory responses elevate pro-inflammatory cytokines while concurrently suppressing the activity of systemic anti-inflammatory cytokines. This resulted in a significant rise ($p < 0.05$) in serum TNF-α, IL-1β, and IL-6 levels compared with the sham group, along with a notable decline ($p < 0.05$) in IL-10 and IL-4. In the IS/R + 25 PLRE group, PLRE treatment lowered serum TNF-α and IL-6 relative to the IS/R group, though the reduction did not reach statistical significance ($p > 0.05$), suggesting PLRE's strong anti-inflammatory effects. Additionally, PLRE treatment progressively increased IL-10 and IL-4 levels while decreasing pro-inflammatory cytokines (IL-1β, TNF-α, and IL-6). These effects were markedly pronounced ($p < 0.05$) when PLRE was administered at 50 mg/kg in the IS/R + 50 PLRE group compared with the IS/R group (Fig. 4b).

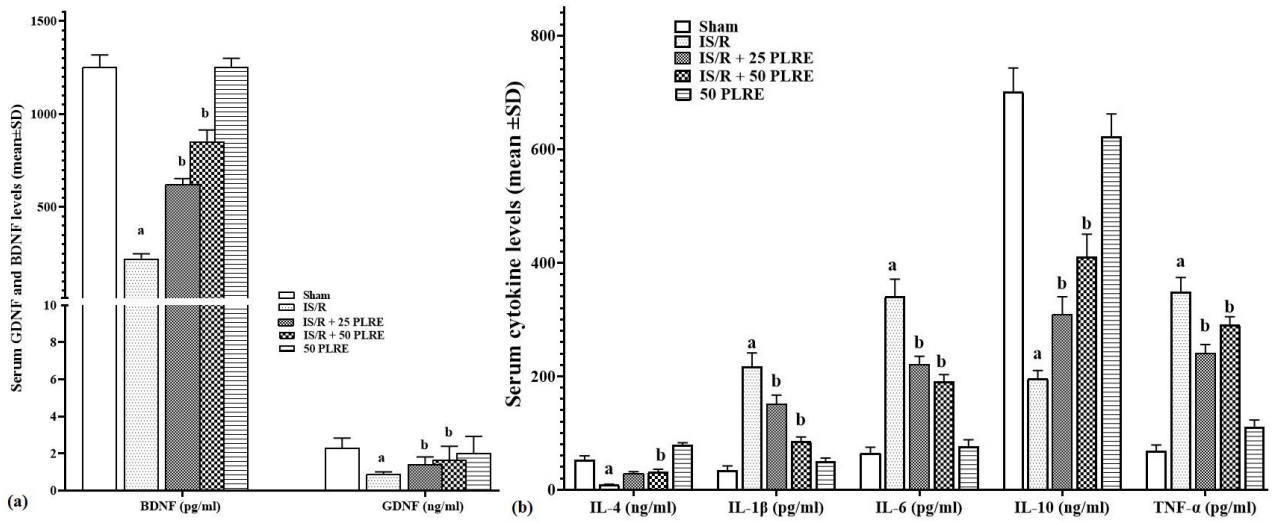

Fig. 4. Serum biomarker profile of (a) neurotrophic factors (GDNF [ng/mL] and BDNF [pg/mL]) and (b) inflammatory mediators (pro-inflammatory: IL-1β, TNF-α, IL-6 [pg/mL]; anti-inflammatory: IL-10, IL-4 [ng/mL]) across experimental groups (mean ± SD; n=10). (a) The number of crossing and (b) Escape latency (s) (means ± SD; n=10/group) in experimental groups. a ($p<0.05$) IS/R *vs.* sham groups; b ($p<0.05$) 25 and 50 mg/kg PLRE treated *vs*. IS/R groups.

PLRE and IS/R effects on serum GPx, CAT, and SOD activity alongside serum NO levels

IS/R stimulated free radical production, resulting in a notable rise in serum nitric oxide (NO) levels relative to the sham group. By contrast, PLRE treatment in the IS/R + 25 and IS/R + 50 groups reduced NO concentrations compared with the IS/R group. Both the 25 and 50 PLRE doses significantly lowered serum NO levels ($p < 0.05$), underscoring PLRE's robust antioxidant properties. Additionally, IS/R markedly decreased the serum activities of all three antioxidant enzymes when compared with sham animals. In contrast, PLRE at 25 and 50 mg/kg increased these enzyme levels, with a significant elevation ($p < 0.05$) in the IS/R + 25 and IS/R + 50 groups versus the IS/R group (Fig. 5a).

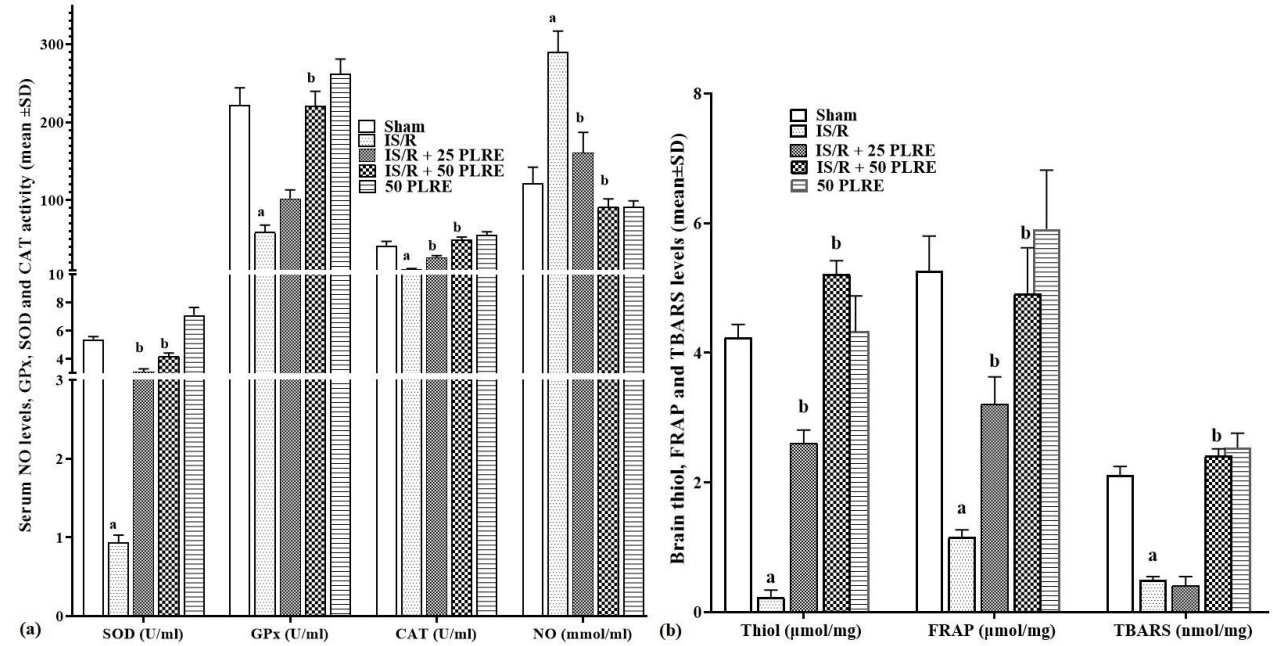

Fig. 5. Oxidative stress modulation profile: (a) Serum nitric oxide (NO) concentration (mmol/mL) and antioxidant enzyme activities (SOD, CAT, GPx; U/mL) (b) Brain tissue oxidative damage markers: TBARS (lipid peroxidation, nmol/mg), thiol content (sulfhydryl groups, µmol/mg), and FRAP assay (antioxidant capacity, µmol/mg) across experimental groups (mean ± SD; n=10). a ($p<0.05$) IS/R *vs.* sham groups; b ($p<0.05$) 25 and 50 mg/kg PLRE treated vs. IS/R groups.

PLRE and IS/R effects on brain thiol, FRAP, and TBARS levels

Levels of thiols, FRAP, and TBARS were evaluated as key indicators of total antioxidant capacity and lipid peroxidation (LPO), and the results showed that IS/R markedly ($p < 0.05$) reduced these markers in tissue relative to the sham group; conversely, the robust antioxidant effects of PLRE led to higher marker levels in the IS/R + 25 and IS/R + 50 groups compared with the IS/R group (Fig. 5b).

PLRE and IS/R effects on expression of brain JNK, TLR4, T3JAM, ASK1, GRP78, and ATF-6 genes

Gene expression profiling of apoptosis, oxidative stress, and metabolic pathways in glial and neural cells revealed that IS/R significantly upregulated JNK, TLR4, T3JAM, and ASK1, while ATF-6 and GRP78 levels were notably reduced in the brain relative to the sham group ($p < 0.05$). The most substantial effects occurred in the IS/R + 50 group, where the expressions of JNK, TLR4, T3JAM, and ASK1, as well as ATF-6 and GRP78, were significantly lower than in the IS/R group ($p < 0.05$), implicating TLR4/T3JAM- and ASK1-related inflammatory signaling pathways (Fig. 6).

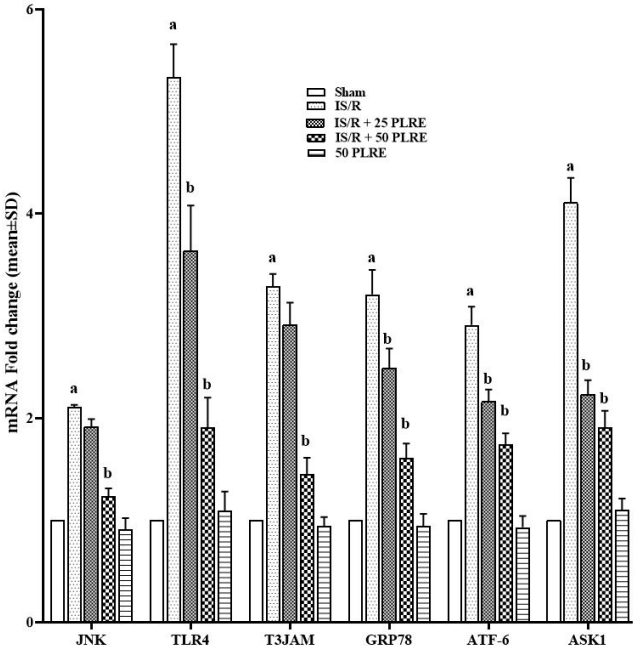

Fig. 6. Molecular mechanisms of ischemia-reperfusion injury and PLRE-mediated neuroprotection: inflammatory markers JNK, TLR4, T3JAM, ASK1 and endoplasmic reticulum stress markers (ATF-6/GRP78) in brain tissue (mean ± SD; n=10/group). a ($p<0.05$) IS/R *vs*. sham groups; b ($p<0.05$) 25 and 50 mg/kg PLRE treated *vs*. IS/R groups.

Brain streological and histopathological evaluations

IS/R injury significantly ($p < 0.05$) reduced total brain (TBV) and neuronal parenchyma tissue (NPTV) volume while significantly ($p < 0.05$) increasing blood vessels (BVV) and ischemic foci (FIV) volume compared to sham controls, mediated through heightened neuroinflammation and structural damage to both neuronal and glial components; however, treatment with PLRE, particularly at the 50 mg/kg dose (IS/R + 50 PLRE group), demonstrated significant neuroprotective efficacy ($p < 0.05$) by attenuating inflammatory responses, preserving parenchymal integrity, and partially reversing vascular abnormalities, ultimately showing significant mitigation of IS/R-induced volumetric changes and pathological markers relative to untreated IS/R subjects (Fig. 7).

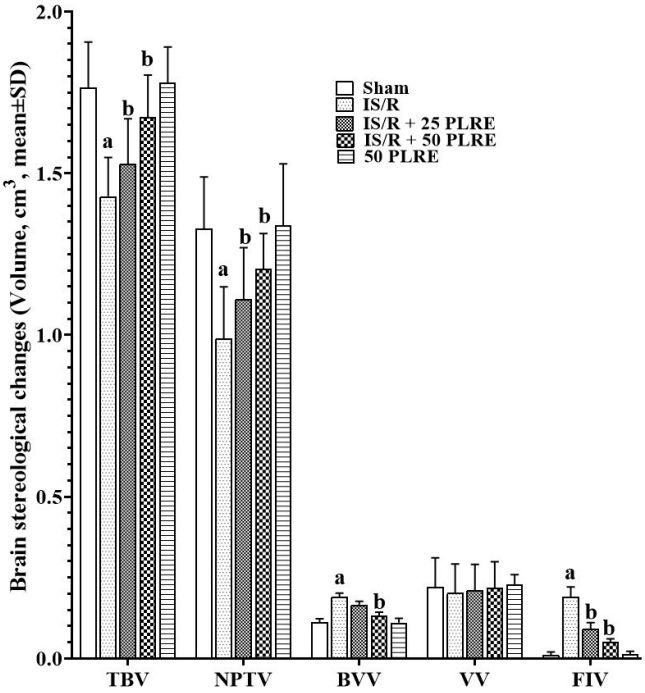

Fig. 7. Stereological changes in brain tissue across experimental groups(mean ± SD; n=10/group). a ($p<0.05$) IS/R vs. sham groups; b ($p<0.05$) 25 and 50 mg/kg PLRE treated *vs*. IS/R groups. Total brain (TBV), neuronal parenchyma tissue (NPTV), blood vessels (BVV), and ischemic foci (FIV) volume.

Histopathological examination of brain tissue showed that IS/R induced lymphocytic infiltration (LI), vascular damage, neurons with pyknotic nuclei and vacuolated cytoplasm, apoptotic bodies (AP), and degenerated neurons near necrotic zones (N), with the IS/R group exhibiting pronounced neuronal atrophy and a substantial decrease in normal parenchymal density relative to the sham group. In contrast, PLRE treatment in the IS/R + 25 and IS/R + 50 PLRE groups increased neuronal

parenchymal density and markedly reduced apoptotic bodies, neuronal degeneration, and LI compared with the IS/R group (Fig. 8a).

TEM findings

Electron microscopic analysis revealed distinct ultrastructural differences between groups: Sham group neurons exhibited large euchromatic nuclei with dispersed chromatin and prominent nucleoli, accompanied by mitochondria displaying intact cristae, extensive rough endoplasmic reticulum forming Nissl bodies, perinuclear Golgi complexes with vesicular budding, and myelinated axons (12-15 myelin lamellae) supported by dense neurofilament networks. In contrast, IS/R group neurons showed pathological alterations including shrunken nuclei with heterochromatin condensation, swollen mitochondria with cristae disruption, lysosomal proliferation, apoptotic vesicles, and structural degradation of neurofilaments and myelin sheaths. PLRE-treated groups (particularly IS/R + 50 PLRE) demonstrated significant neuroprotection, with preserved euchromatic nuclear morphology, mitochondrial integrity, reduced lysosomal counts, absence of apoptotic vesicles, and maintained glial foot process architecture, indicating dose-dependent mitigation of ischemia-reperfusion-induced damage (Fig. 8b).

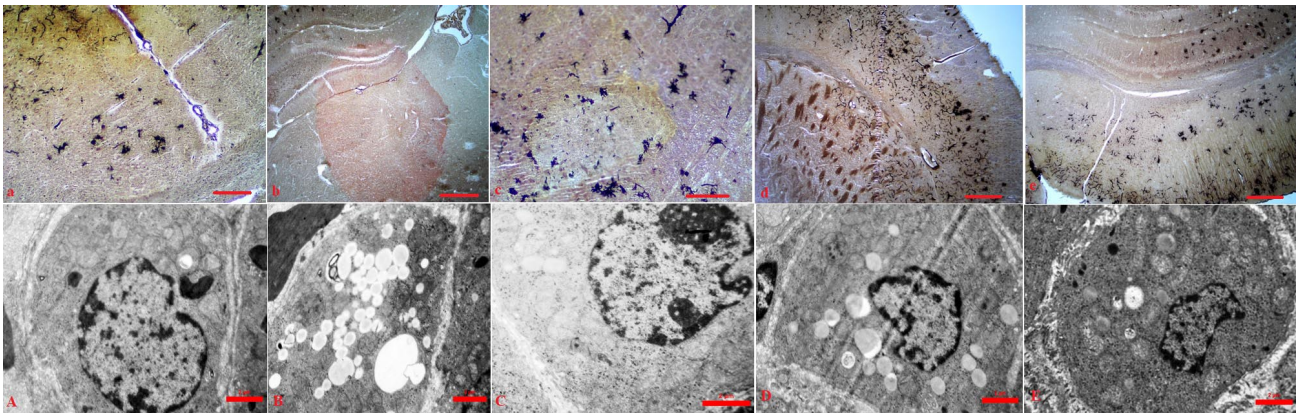

Fig. 8. Upper raw: Histopathological changes in brain tissue in (a) Sham, (b) IS/R, (c) IS/R + 25 mg/kg PLRE, (d) IS/R + 50 mg/kg PLRE, and (e) 50 mg/kg PLRE alone (Golgi's staining × 100 with scale bar = 200 µm). Lower raw: TEM micrographs of the brain tissue in in (A) Sham, (B) IS/R, (C) IS/R + 25 mg/kg PLRE, (D) IS/R + 50 mg/kg PLRE, and (E) 50 mg/kg PLRE alone (Scale bar = 2 µm).

DISCUSSION

The neuroprotective efficacy of PLRE against CI/R injury is robustly demonstrated in this study, with 50 mg/kg PLRE significantly ameliorating cognitive deficits and neuronal damage in a rat MCAO model. Spatial learning and memory impairments, quantified through Morris water maze testing, were markedly reversed by PLRE treatment, evidenced by reduced escape latency and increased platform crossings. This cognitive restoration correlates with elevated serum levels of neurotrophic factors BDNF and GDNF, which are crucial for synaptic plasticity and neuronal survival (Nicoletti *et al*., 2022). Histopathological analyses further support these findings, showing PLRE's dose-dependent preservation of neuronal parenchymal volume, reduction in apoptotic bodies, and attenuation of degenerative changes like pyknotic nuclei and vacuolated cytoplasm. These outcomes align with PLRE's established anti-apoptotic properties, likely mediated through modulation of Bax/Bcl-2 pathways and caspase-3 inhibition, thereby maintaining structural and functional integrity in vulnerable hippocampal and cortical regions. The 50 mg/kg dose emerged as particularly efficacious, underscoring PLRE's potential to enhance post-stroke neuroregeneration beyond mere symptom management.

Central to PLRE's mechanism is its suppression of JNK-mediated inflammatory cascades, which critically exacerbate CI/R injury. The extract significantly downregulated key upstream activators of JNK phosphorylation, including TLR4, T3JAM, and ASK1, disrupting the TLR4/MyD88/TRIF signaling axis that drives NF-kB translocation and pro-inflammatory cytokine production. This inhibition translated to reduced serum levels of TNF-a, IL-1b, and IL-6, alongside normalized anti-inflammatory markers IL-10 and IL-4, indicating a shift toward protective microglial polarization (Wu *et al*., 2025). Crucially, immunohistochemistry revealed diminished JNK-positive cells in PLRE-treated groups, corroborating the gene expression data. By targeting multiple nodes of the JNK pathway—such as TLR4/T3JAM-dependent signaling and ASK1-induced oxidative stress responses—PLRE achieves

broader anti-inflammatory effects than selective JNK inhibitors. This multi-target action mitigates downstream pathologies like blood-brain barrier disruption and COX-2 overexpression, positioning PLRE as a holistic modulator of neuroinflammation in the ischemic penumbra (Xu *et al*., 2021).

PLRE further demonstrated potent antioxidant and endoplasmic reticulum (ER) stress-regulating properties, essential for countering CI/R-induced oxidative damage. Treatment restored glutathione peroxidase (GPx), superoxide dismutase (SOD), and catalase (CAT) activities, directly scavenging reactive oxygen species (ROS) and reducing serum nitric oxide (NO) levels—a key mediator of lipid peroxidation. Concurrently, diminished thiobarbituric acid-reactive substances (TBARS) and elevated thiol content in brain tissue confirmed PLRE's capacity to curb membrane degradation. Equally significant was the upregulation of ER chaperones GRP78 and ATF-6, which alleviate unfolded protein response (UPR)-driven apoptosis by inhibiting effectors like CHOP and caspase-12 (Das *et al*.,2023). Phytochemical analysis identified bioactive constituents such as biochanin A, apigenin, and quercetin in PLRE, which likely potentiate these effects via Nrf2/ARE pathway activation (Huang *et al*., 2023; Aleksandrs, 2024). This dual antioxidant-ER stress modulation not only preserves cellular homeostasis but also synergizes with PLRE's anti-inflammatory actions, creating a comprehensive defense against the multifactorial pathology of ischemic injury.

The translational promise of PLRE is underscored by stereological data showing reduced infarct volume and normalized microvascular architecture at 50 mg/kg, suggesting vascular protection alongside neuronal salvage. However, the absence of a linear dose-response gradient between 25 mg/kg and 50 mg/kg in some parameters warrants exploration of optimal dosing, while the study's acute-phase focus(24–72 hours post-reperfusion) leaves long-term neurogenesis and functional recovery unaddressed. Future research should prioritize pharmacokinetic profiling to assess blood-brain barrier penetration of PLRE compounds and evaluate combinatorial therapies with thrombolytics like tPA (Chen *et al*., 2022). Clinically, PLRE's natural origin and multi-target efficacy could extend the narrow treatment window for ischemic stroke, particularly in resource-limited settings. Nevertheless, rigorous human trials are needed to validate efficacy, standardize extracts, and identify potential herb-drug interactions. This study lays a robust preclinical foundation for PLRE as a disease-modifying adjunct in stroke management, bridging traditional phytomedicine with contemporary neuroprotection paradigms.

This study conclusively demonstrates that PLRE at 50 mg/kg exerts potent neuroprotective effects in a rat model of cerebral ischemia-reperfusion injury, significantly mitigating cognitive deficits, reducing infarct volume, and attenuating neuroinflammation through the suppression of JNK-mediated TLR4/T3JAM- and ASK1-dependent inflammatory signaling pathways. By enhancing antioxidant enzyme activity (SOD, CAT, GPx), restoring neurotrophic factor levels (BDNF, GDNF), and modulating endoplasmic reticulum stress markers (GRP78, ATF-6), PLRE addresses the multifactorial pathology of ischemic injury, offering a multi-target therapeutic strategy that outperforms conventional single-pathway interventions. The LC-ESI/MS-identified bioactive compounds, including biochanin A and apigenin, likely underpin these effects, synergistically combating oxidative stress, apoptosis, and microglial hyperactivation. These findings position PLRE as a promising natural adjuvant for ischemic stroke management, warranting further clinical trials to validate its translational potential and optimize dosing regimens for human applications.

Ethical Approval. The experimental protocols of this study were approved by the Hubei University of Medicine ethics committee.

LI, Z-F.; ZHAO, Y-Y.; ZHANG, Y-Q. & ZHU, Z-R. Efectos del extracto de raíz de *Paeonia lactiflora* sobre la señalización inflamatoria mediada por JNK y la reducción del infarto cerebral en la isquemia focal transitoria aguda en ratas. *Int. J. Morphol., 44(1)*:325-339, 2026.

RESUMEN: La lesión por isquemia-reperfusión cerebral (IC/R) compromete significativamente las capacidades cognitivas tras un infarto cerebral (IC). Esta investigación estudió el impacto del extracto de raíz de *Paeonia lactiflora* L. (ERPL) en un modelo de IC/R utilizando ratas Wistar, así como los mecanismos implicados. Un total de cincuenta ratas Wistar fueron asignadas aleatoriamente a cinco grupos: un grupo control, un grupo suplementado con 50 mg/kg de PLRE, un grupo CI y dos grupos CI tratados con 25 mg/kg y 50 mg/kg de PLRE, cada grupo compuesto por 10 ratas. La función cognitiva se evaluó mediante la prueba del laberinto en Y. Además, utilizamos el ensayo inmunoenzimático (ELISA) y la PCR en tiempo real para analizar la expresión de genes vinculados a la apoptosis mediada por JNK, TLR4/T3JAM y la señalización inflamatoria relacionada con ASK1 en el cerebro. En comparación con el grupo control, el grupo CI mostró un retraso significativo en la finalización del laberinto ($p<0,05$). Este grupo también presentó niveles significativamente más altos de citocinas proinflamatorias, junto con niveles reducidos de citocinas antiinflamatorias y factores de crecimiento neurotróficos [factor neurotrófico derivado del cerebro (BDNF) y factor neurotrófico derivado de la línea celular glial (GDNF)] ($p<0,05$). Por el contrario, el grupo tratado con 50 mg/kg de PLRE después de la lesión cerebral traumática (LCT) mostró mejoras, incluyendo una reducción del tiempo de estimulación eléctrica,

niveles elevados de factores de crecimiento neurotróficos y una alteración beneficiosa en los perfiles de expresión de genes relacionados con la inflamación y la apoptosis (como la proteína 78 regulada por glucosa (GRP78), el factor de transcripción activador 6 (ATF-6), TLR4, T3JAM y ASK1) en comparación con el grupo LCT ($p<0,05$). Estos hallazgos indican que el extracto de PLRE podría aliviar los déficits cognitivos posteriores a la LCT en ratas, posiblemente modulando los factores inflamatorios secretados por la microglia.

PALABRAS CLAVE: *Paeonia lactiflora* L.; Infarto cerebral; Apoptosis; Isquemia-reperfusión cerebral.

REFERENCES

Aleksandrs, R. The impact of telerehabilitation therapies and information and communication technology on stroke recovery. *Int. J. Clin. Med. Res., 2(6)*:214-20, 2024.

Chen, S.; Zhang, J.; Li, M.; Zhou, J. & Zhang, Y. Danhong injection combined with tPA protects the BBB through Notch-VEGF signaling pathway on long-term outcomes of thrombolytic therapy. *Biomed. Pharmacother., 153*:113288, 2022.

Cheng, C. Y.; Chiang, S. Y.; Kao, S. T. & Huang, S. C. Alpinia oxyphylla Miq extract reduces cerebral infarction by downregulating JNK-mediated TLR4/T3JAM- and ASK1-related inflammatory signaling in the acute phase of transient focal cerebral ischemia in rats. *Chin. Med., 16(1)*:82, 2021.

Choi, M. Y.; Park, S. J. & Jeong, J. B. Immunostimulatory activity of *Paeonia lactiflora* through TLR4-dependent activation of p38, JNK, and ERK1/2 in mouse macrophages RAW264.7 cells. *Food Agric. Immunol., 34(1)*:2222930, 2023.

Das, B.; Samal, S.; Hamdi, H.; Pal, A.; Biswas, A.; Behera, J.; Singh, G.; Behera, C. K.; Sahoo, D. P. & Pati, S. Role of endoplasmic reticulum stress-related unfolded protein response and its implications in dengue virus infection for biomarker development. *Life Sci., 329*:121982, 2023.

Goodarzi, N.; Akbari Bazm, M.; Poladi, S.; Rashidi, F.; Mahmoudi, B. & Abumandour, M. M. Histology of the small intestine in the common pheasant (*Phasianus colchicus*): A scanning electron microscopy, histochemical, immunohistochemical, and stereological study. *Microsc. Res. Tech., 84(10)*:2388-98, 2021.

Huang, W.; Zhong, Y.; Gao, B.; Zheng, B. & Liu, Y. Nrf2-mediated therapeutic effects of dietary flavones in different diseases. *Front. Pharmacol., 14*:1240433, 2023.

Khazaei, F.; Naseri, L.; Akbaribazm, M. & Khazaei, M. Foeniculum vulgare extract enhances estrogen levels, total antioxidant capacity, and protects ovarian histology in rats exposed to bisphenol A. *Endocrinol. Res. Pract., 27(4)*:227-32, 2023.

Khazayel, S.; Faraji, M. H.; Akbaribazm, M.; Khazaei, M.; Niromand, E. & Khazaei, M. R. Synergistic inhibitory effects of *Trifolium pratense* L. extract and doxorubicin on 4T1 tumor-bearing mice are mediated via targeting the Wnt/b-catenin pathway and reversal of epithelial-mesenchymal transition. *Avicenna J. Phytomed., 15(5)*:1546-61, 2025.

Khordad, E.; Akbaribazm, M. & Hosseini, S. M. Heracleum persicum L. extract protects gentamicin-induced testicular toxicity. *Avicenna J. Phytomed., 14(5)*:585-99, 2024.

Kim, J.; Thayabaranathan, T.; Donnan, G. A.; Howard, G.; Howard, V. J.; Rothwell, P. M.; Feigin, V.; Norrving, B.; Owolabi, M.; Pandian, J.; *et al*. Global stroke statistics 2019. *Int. J. Stroke, 15(8)*:819-38, 2020.

Kim, M. J.; Kang, H. H.; Seo, Y. J.; Kim, K. M.; Kim, Y. J. & Jung, S. K. *Paeonia lactiflora* root extract and its components reduce biomarkers of early atherosclerosis via anti-inflammatory and antioxidant effects in vitro and in vivo. *Antioxidants (Basel), 10(10)*:1507, 2021.

Kulshrestha, A.; Katara, G. K.; Ibrahim, S. A.; Riehl, V.; Sahoo, M.; Dolan, J.; Meinke, K. W.; Pins, M. R. & Beaman, K. D. Targeting V-ATPase isoform restores cisplatin activity in resistant ovarian cancer: inhibition of autophagy, endosome function, and ERK/MEK pathway. *J. Oncol., 2019*:2343876, 2019.

Li, X. Q.; Wang, J.; Fang, B.; Tan, W. F. & Ma, H. Intrathecal antagonism of microglial TLR4 reduces inflammatory damage to blood–spinal cord barrier following ischemia/reperfusion injury in rats. *Mol. Brain, 7*:28, 2014.

Liang, T.; Xu, S.; Liu, R. & Xia, X. Activating transcription factor 6 alleviates secondary brain injury by increasing cystathionine g-lyase expression in a rat model of intracerebral hemorrhage. *Aging (Albany NY), 16(8)*:6990-7008, 2024.

Ma, B. & Wang, R. Therapeutic potential of hydroalcoholic extract of Rumex alveollatus L. leaves in atherosclerosis: Biochemical, molecular, and histopathological insights from a rat model. *Pharmacogn. Mag., 2025*. Doi: 10.1177/09731296251350747

Ma, Y. T.; Li, C.; Shen, Y.; You, W. H.; Han, M. X.; Mu, Y. F. & Han, F. J. Mechanisms of the JNK/p38 MAPK signaling pathway in drug resistance in ovarian cancer. *Front. Oncol., 15*:1533352, 2025.

Meng, C.; Zhang, J.; Zhang, L.; Wang, Y.; Li, Z. & Zhao, J. Effects of NLRP6 in cerebral ischemia/reperfusion (I/R) injury in rats. *J. Mol. Neurosci., 69(3)*:411-8, 2019.

Mohsen, A.; Fatemeh, K.; Leila, N.; Mona, P.; Mohammad, Z. & Mozafar, K. Pharmacological and therapeutic properties of the Red Clover (*Trifolium pratense* L.): an overview of the new finding. *J. Tradit. Chin. Med., 41(4)*:642-9, 2021.

Ni, M.; Zhang, Y. & Lee, A. S. Beyond the endoplasmic reticulum: atypical GRP78 in cell viability, signalling and therapeutic targeting. *Biochem. J., 434(2)*:181-8, 2011.

Nicoletti, V. G.; Pajer, K.; Calcagno, D.; Pajenda, G. & Nógrádi, A. The role of metals in the neuroregenerative action of BDNF, GDNF, NGF and other neurotrophic factors. *Biomolecules, 12(8)*:1015, 2022.

Owolabi, M. O.; Thrift, A. G.; Martins, S.; Johnson, W.; Pandian, J.; Abd-Allah, F.; Varghese, C.; Mahal, A.; Yaria, J.; Phan, H. T.; *et al*. The state of stroke services across the globe: report of World Stroke Organization–World Health Organization surveys. *Int. J. Stroke, 16(8)*:889-901, 2021.

Soleimani, N.; Keshtmand, Z.; Goodarzi, N. & Akbaribazm, M. Phytofabricated silver nanoparticles from *Vaccinium arctostaphylos* L.: Anticancer activity against breast cancer cells via apoptosis induction and growth suppression. *Food Sci. Nutr., 13(11)*:e71202, 2025.

Su, Q.; Li, L.; Sun, Y.; Yang, H.; Ye, Z. & Zhao, J. Effects of the TLR4/Myd88/NF-kB signaling pathway on NLRP3 inflammasome in coronary microembolization-induced myocardial injury. *Cell. Physiol. Biochem., 47(4)*:1497-508, 2018.

Sun, Y. Y.; Zhu, H. J.; Zhao, R. Y.; Zhou, S. Y.; Wang, M. Q.; Yang, Y. & Guo, Z. N. Remote ischemic conditioning attenuates oxidative stress and inflammation via the Nrf2/HO-1 pathway in MCAO mice. *Redox Biol., 66*:102852, 2023.

Tunca, Z.; Ozerdem, A.; Ceylan, D.; Yalçın, Y.; Can, G.; Resmi, H.; Akan, P.; Ergör, G.; Aydemir, O.; Cengisiz, C.; *et al*. Alterations in BDNF (brain derived neurotrophic factor) and GDNF (glial cell line-derived neurotrophic factor) serum levels in bipolar disorder: the role of lithium. *J. Affect. Disord., 166*:193-200, 2014.

Wen, S. Y.; Wu, Y. S.; Liu, H.; Ng, S. C.; Padma, V. V.; Huang, C. Y. & Kuo, W. W. Paeoniflorin found in *Paeonia lactiflora* root extract inhibits melanogenesis by regulating melanin-related signal transduction in B16F10 cells. *J. Cosmet. Dermatol., 22(10)*:2824-30, 2023.

Wu, X.; He, T.; Yang, C.; Xue, S.; Yuan, Q.; Chen, F.; Liu, J. & Li, G. Suppressing TLR4 alleviates cerebral injury in heatstroke rats through the modulation of microglial polarization. *Int. J. Hyperthermia, 42(1)*:2503312, 2025.

Xu, X.; Huang, H.; Tu, Y.; Sun, J.; Xiong, Y.; Ma, C.; Qin, S.; Hu, W. & Zhou, J. Celecoxib alleviates radiation-induced brain injury in rats by maintaining the integrity of blood-brain barrier. *Dose Response, 19(2)*:15593258211024393, 2021.

Yang, Y.; Ren, Z. & Xu, J. Synergistic effects of Lactiplantibacillus plantarum GUANKE and tryptophan on alleviating lung injury through the AHR/STAT3/IL-10 pathway in influenza infection mice. *J. Nutr. Biochem., 148*:110165, 2026.

Yu, Q.; Li, G.; Ding, Q.; Tao, L.; Li, J.; Sun, L.; Sun, X. & Yang, Y. Irisin protects brain against ischemia/reperfusion injury through suppressing TLR4/MyD88 pathway. *Cerebrovasc. Dis., 49(4)*:346-54, 2020.

Yuan, J.; Li, L.; Yang, Q.; Ran, H.; Wang, J.; Hu, K.; Pu, W.; Huang, J.; Wen, L.; Zhou, L.; *et al*. Targeted treatment of ischemic stroke by bioactive nanoparticle-derived reactive oxygen species responsive and inflammation-resolving nanotherapies. *ACS Nano, 15(10)*:16076-94, 2021.

Zhang, J. & Dong, B. Effects of *Vaccinium arctostaphylos* L. seeds oil on the cerebral stroke in rat: A biochemical, immunohistochemically and molecular approach. *Int. J. Morphol., 42(6)*:1773-82, 2024.

Zhang, Y.; Zhang, H.; Zhao, F.; Jiang, Z.; Cui, Y.; Ou, M.; Mei, L. & Wang, Q. Mitochondrial-targeted and ROS-responsive nanocarrier via nose-to-brain pathway for ischemic stroke treatment. *Acta Pharm. Sin. B, 13(12)*:5107-20, 2023.

Zhu, W.; Davis, C. M.; Allen, E. M.; Feller, S. L.; Bah, T. M.; Shangraw, R. E.; Wang, R. K. & Alkayed, N. J. Sex difference in capillary reperfusion after transient middle cerebral artery occlusion in diabetic mice. S*troke, 54(2)*:364-73, 2023.

Corresponding author:
Dr. Zhuo-Ran Zhu
Department of Anatomy
Basic Medical College
Hubei University of Medicine
Shiyan, 442000
CHINA

E-mail: zhu25988685@outlook.com

ORCID ID: 0009-0007-6861-1464